


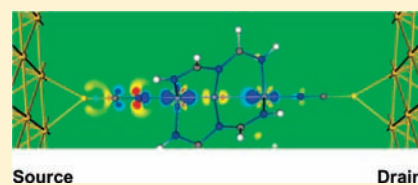
# Influence of Low-Symmetry Distortions on Electron Transport through Metal Atom Chains: When Is a Molecular Wire Really “Broken”?

Vihar P. Georgiev and John E. McGrady\*

Department of Chemistry, Inorganic Chemistry Laboratory, University of Oxford, South Parks Road, Oxford OX1 3QR, United Kingdom

 Supporting Information

**ABSTRACT:** In the field of molecular electronics, an intimate link between the delocalization of molecular orbitals and their ability to support current flow is often assumed. Delocalization, in turn, is generally regarded as being synonymous with structural symmetry, for example, in the lengths of the bonds along a molecular wire. In this work, we use density functional theory in combination with nonequilibrium Green's functions to show that precisely the opposite is true in the extended metal atom chain  $\text{Cr}_3(\text{dpa})_4(\text{NCS})_2$  where the delocalized  $\pi$  framework has previously been proposed to be the dominant conduction pathway. Low-symmetry distortions of the  $\text{Cr}_3$  core do indeed reduce the effectiveness of these  $\pi$  channels, but this is largely irrelevant to electron transport at low bias simply because they lie far below the Fermi level. Instead, the dominant pathway is through higher-lying orbitals of  $\sigma$  symmetry, which remain essentially unperturbed by even quite substantial distortions. In fact, the conductance is actually increased marginally because the  $\sigma^{\text{nb}}$  channel is displaced upward toward the Fermi level. These calculations indicate a subtle and counterintuitive relationship between structure and function in these metal chains that has important implications for the interpretation of data emerging from scanning tunnelling and atomic force microscopy experiments.



## INTRODUCTION

In the rapidly developing field of molecular electronics,<sup>1,2</sup> the search for nanoscale analogues of the wires, diodes, and transistors that make up the fundamental components of electrical circuits is a central theme. Much of the work in this area has focused on conjugated organic systems, where the  $\pi$  framework provides a natural pathway for transfer of electrons.<sup>3</sup> Molecules featuring chains of transition metal atoms have, in contrast, received rather less attention despite their appealing, if perhaps superficial, resemblance to macroscopic wires. The compact *nd* orbitals, particularly those of the first transition series, favor the adoption of nonsinglet states, offering the possibility of spin-polarized currents.<sup>4</sup> For example, both da Silva<sup>5</sup> and Sanvito<sup>6</sup> have shown that even a single cobalt center can act as an effective spin filter due to the alignment of the partially occupied spin- $\beta$  components of the *d* orbitals with the Fermi level. Isolated atoms are, however, intrinsically difficult to manipulate, and stable coordination complexes clearly offer much greater potential for control and tuning of the density of states around the Fermi level. Baranger and Yang<sup>7</sup> have recently illustrated how a cobaltocene unit can act similarly as an efficient spin filter, and transport through metalloporphyrin<sup>8</sup> and phthalocyanine<sup>9</sup> units has also been explored in some detail. Das has also noted the possibility of using coordination-induced changes in the conductance of ligands as a sensing mechanism.<sup>10</sup> Arrays of metal ions linked by bridging ligands represent a logical step toward true molecular “wires”,<sup>11</sup> and the sandwich complexes  $[\text{ML}]_n$ , where L is an

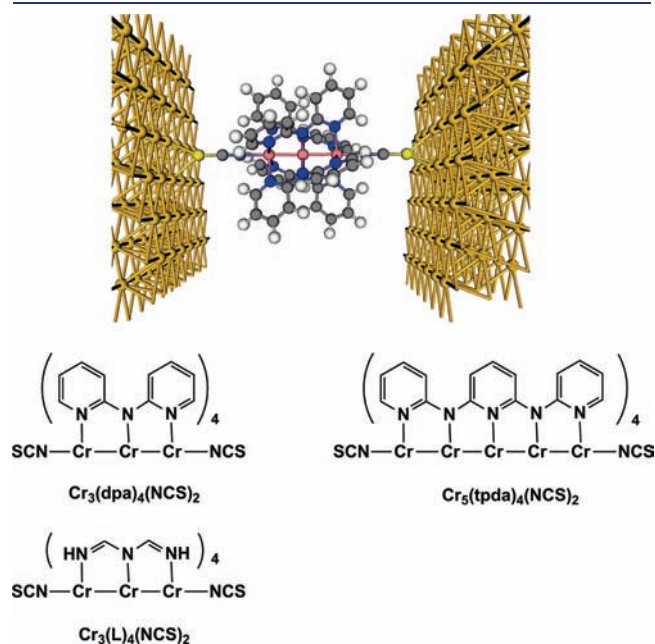
aromatic ligand such as cyclopentadienyl,<sup>12–14</sup> benzene,<sup>15</sup> borazine,<sup>16</sup> borolyl,<sup>17</sup> or cyclooctatetraenyl,<sup>18</sup> have been extensively studied in this context. The interactions between metal ions in such arrays offer a mechanism for controlling electron transport through switching between ferro- and antiferromagnetic states, and in dicobaltocene systems the former is substantially more transparent than the latter.<sup>19</sup> “Magnetic superatoms” such as  $\text{VCs}_8$ <sup>20</sup> have also been shown to provide a basis for significant spin filtering.<sup>21</sup> Electron transport through three-dimensional arrays of paramagnetic centers in single molecule magnets (SMMs)<sup>22–26</sup> has also been discussed in the recent literature, and bias-induced rehybridization of orbitals has been shown to have a substantial impact on the transmission channels in a  $\text{Mn}_{12}$  cluster.<sup>27</sup>

In all of the polymetallic complexes noted in the previous paragraph, the metal ions are linked indirectly via exchange coupling. Systems where direct covalent bonds are present between the metals have, in contrast, received less attention. There have been numerous discussions of electron transport through “bare” atomic wires<sup>28</sup> and also chains absorbed on or in carbon nanotubes,<sup>29</sup> but again these offer limited potential for control at the synthetic level. Among the few truly molecular examples, Berber and co-workers have explored transport through octahedral  $\text{Mo}_6$  clusters,<sup>30</sup> while Huang et al. have

Received: March 29, 2011

Published: July 12, 2011

shown that the linear and *trans*-bent isomers of quintuple Cr–Cr bonds<sup>31,32</sup> can support on/off current ratios ( $I_{trans-bent}/I_{linear}$ ) of the order of 100.<sup>33</sup> The family of extended metal atom chains (EMACs), based on helical arrays of polypyridylamido ligands (Figure 1), provides a particularly striking resemblance to a macroscopic wire. The chemistry of these systems has been developed extensively in the groups of Peng<sup>34</sup> and Berry, Cotton, and Murillo,<sup>35,36</sup> and chains containing up to nine metal atoms<sup>37</sup> are now well characterized. More importantly, in the context of electron transport, examples are known for metals with widely



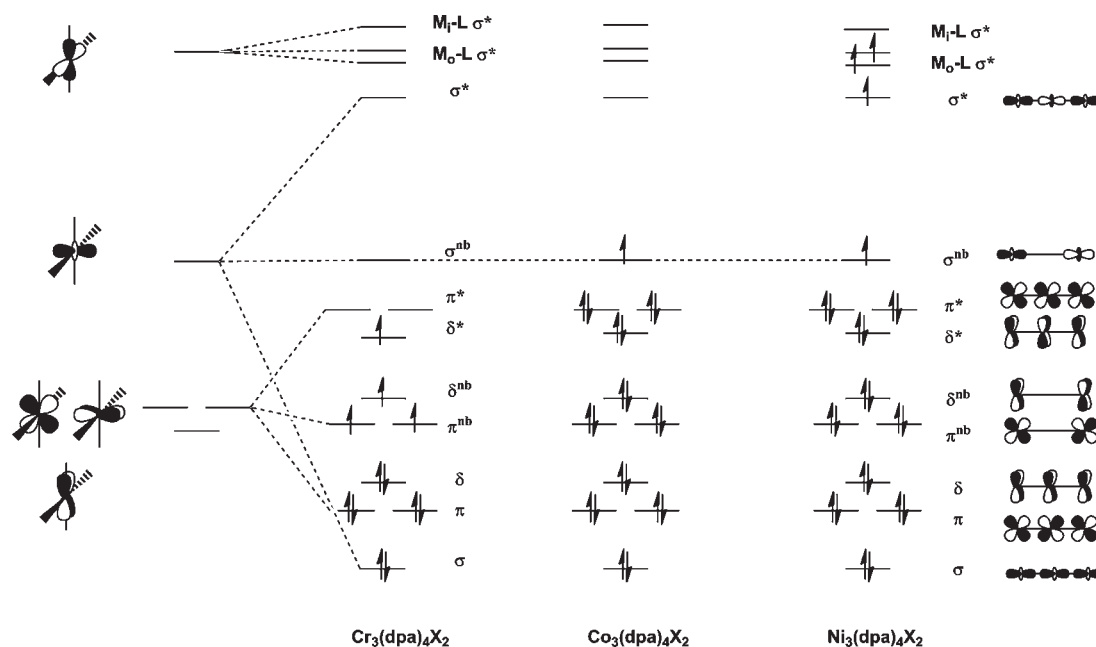
**Figure 1.** Structures of the two-probe arrangement, the  $\text{Cr}_3(\text{dpa})_4(\text{NCS})_2$  and  $\text{Cr}_5(\text{tpda})_4(\text{NCS})_2$  EMACs, and the model complex  $\text{Cr}_3(\text{L})_4(\text{NCS})_2$  (color scheme: pink, Cr; blue, N; gray, C; yellow, S; white, H).

differing d-electron counts and therefore metal–metal bond types. The structural and magnetochemical properties<sup>38</sup> of the  $\text{Co}_3(\text{dpa})_4\text{Cl}_2$  chains (dpa = dipyridylamide) are particularly intriguing as the molecule exists in two quite distinct forms where the lengths of the Co–Co and Co–N bonds are very different.<sup>39–41</sup> We have recently shown that this remarkable structural chemistry can be understood in terms of a rather complex temperature-dependent redistribution of charge density between the  $\sigma$ ,  $\pi$ , and  $\delta$  components of the Co–Co–Co manifold,<sup>42</sup> an observation that leads naturally to the question of how such a system might behave under applied bias in a putative molecular electronic device.

The basic features of the bonding in this class of molecules have been established using symmetry-based arguments (Scheme 1).<sup>35,43,44</sup> If the component metal ions are viewed, to a first approximation, as square planar, then the manifold of metal-based orbitals separates into a lower-lying block consisting of linear combinations of the four approximately M–L nonbonding orbitals ( $d_{xz}$ ,  $d_{xy}$ ,  $d_{yz}$ ,  $d_{z^2}$ ) and an upper block consisting of linear combinations of the M–L antibonding  $d_{x^2-y^2}$  orbitals. The former separates into components with  $\sigma$  ( $d_{z^2}$ ),  $\pi$  ( $d_{xz}$ ,  $d_{yz}$ ), and  $\delta$  ( $d_{xy}$ ) symmetry with respect to the M–M axis. In the  $\text{Co}_3(\text{dpa})_4\text{X}_2$  chain ( $d^7$  configuration), all bonding, nonbonding, and antibonding combinations of  $\pi$  and  $\delta$  symmetry are occupied, as is the  $\sigma$  bonding orbital, leaving a single electron in the  $\sigma$  nonbonding orbital. The net Co–Co bond order is therefore 0.5. In  $\text{Ni}_3$  ( $d^8$ ), the additional three electrons occupy the Ni–Ni  $\sigma^*$  orbital along with two M–N  $\sigma^*$  orbitals localized on the outer Ni atoms. For Cr, however, only 12 valence electrons are available, and a quintet ground state arising from the  $(\sigma)^2(\pi)^4(\delta)^2(\pi^{nb})^2(\delta^{nb})^1(\delta^*)^1$  configuration, with a net Cr–Cr bond order of 1.5, has been proposed.<sup>35,43,44</sup>

Even before the first experimental measurements of electron transport by EMACs, Berry et al. had anticipated potential applications in molecular electronics.<sup>45</sup> Yao and co-workers subsequently went on to explore gated electron transport through both  $\text{Ni}_3(\text{dpa})_4(\text{Cl})_2$  and  $\text{Cu}_3(\text{dpa})_4(\text{Cl})_2$ ,<sup>46</sup> showing clear

**Scheme 1.** Schematic Molecular Orbital Arrays for  $\text{M}_3(\text{dpa})_4\text{X}_2$ , M = Cr, Co, and Ni<sup>35,43</sup>



evidence for Coulomb blockade behavior due to charging of the molecule. Peng and co-workers have used both conductive atomic force microscopy (CAFM) and scanning tunnelling microscopy (STM) techniques to probe the conductance ( $G$ ) of tri- and pentametallic chains,  $M_3(\text{dpa})_4(\text{NCS})_2$  and  $M_5(\text{tpda})_4(\text{NCS})_2$ ,  $M = \text{Cr}, \text{Co}, \text{Ni}$ .<sup>44</sup>  $G$  proves to be highly dependent on the identity of the metal ion, increasing in the order  $\text{Ni}$  ( $0.006 \mu\text{S}$ ) <  $\text{Co}$  ( $0.021 \mu\text{S}$ ) <  $\text{Cr}$  ( $0.37 \mu\text{S}$ ), the variation over 2 orders of magnitude suggesting that electronic configuration plays a critical role in controlling the flow of electrons. The precise link between electronic structure and electron transport is not, however, clear. Intuitively, a more delocalized distribution of electrons might be expected to enhance conductance,<sup>47,48</sup> and Peng and co-workers have argued that the observed trend correlates directly with the changes in formal  $M-M$  bond order captured in Figure 1.<sup>44,49</sup> Moreover, by analogy with organic conductors, it is tempting to suppose that the  $\pi$  bonds present in the  $\text{Cr}_3$  and  $\text{Cr}_5$  chains but not their  $\text{Co}$  or  $\text{Ni}$  analogues are the key difference. However, Bénard and Rohmer's detailed DFT study of the electronic structure of  $\text{Cr}_3(\text{dpa})_4\text{Cl}_2$  suggests a bonding model that differs significantly from that shown in Scheme 1. There is, in fact, very little overlap between the orbitals of  $\pi$  and  $\delta$  symmetry, and as a result all linear combinations ( $\pi$ ,  $\pi^{\text{nb}}$ , and  $\pi^*$  and  $\delta$ ,  $\delta^{\text{nb}}$ , and  $\delta^*$  in Scheme 1) are singly occupied, along with the  $\sigma^{\text{nb}}$  HOMO. The  $\pi$  and  $\delta$  components therefore make a negligible contribution to  $\text{Cr}-\text{Cr}-\text{Cr}$  bonding, which is instead dominated by the 3-center-3-electron  $\sigma$  framework. The electronic structure is therefore qualitatively very similar to that in the  $\text{Co}_3$  analogue, leaving unresolved the issue of the greatly enhanced conductance of the chromium species.<sup>42</sup>

Perhaps even more intriguing than the intrinsically high conductance of the chromium chains is the observation that the pentachromium chain  $\text{Cr}_5(\text{tpda})_4(\text{NCS})_2$  shows evidence for two distinct states, one highly conducting ( $G \approx 0.3 \mu\text{S}$ ), the other less so ( $G \approx 0.068 \mu\text{S}$ ).<sup>44</sup> The absence of detailed information regarding the orientation of the molecules with respect to the electrode surface complicates the interpretation of this bimodality, but the complex structural chemistry of the chromium chains offers one possible explanation. The shorter  $\text{Cr}_3$  chains show a remarkable degree of structural flexibility, and indeed the interpretation of the crystallographic data has been highly controversial. For example, although the dichloromethane solvate of the dichloride capped species  $\text{Cr}_3(\text{dpa})_4\text{Cl}_2 \cdot \text{CH}_2\text{Cl}_2$  was initially reported to be perfectly symmetric ( $\text{Cr}-\text{Cr} = 2.366(1) \text{ \AA}$ ),<sup>50</sup> a subsequent analysis of the effects of disorder revealed a distinct asymmetry in the  $\text{Cr}_3$  core,  $\text{Cr}-\text{Cr} = 2.254(4)$  and  $2.477(4) \text{ \AA}$ .<sup>45</sup> Evidence for a thermal equilibrium between symmetric and unsymmetric isomers in  $\text{Cr}_3(\text{dpa})_4\text{Cl}_2$  has also been presented in the form of strongly temperature dependent surface-enhanced Raman spectra (SERS).<sup>51</sup> Similarly, the NCS-capped analogue is somewhat asymmetric ( $\text{Cr}-\text{Cr} = 2.234(1)$  and  $2.482(1) \text{ \AA}$  in the benzene solvate).<sup>45,52</sup> The degree of asymmetry is inversely correlated to the  $\sigma$  donor strength of the terminal ligands, and only strong  $\sigma$  donors such as  $\text{CN}^-$  or  $\text{CCPh}^-$  yield truly symmetric structures. At the opposite extreme, the  $\text{NO}_3^-$ -capped species has  $\text{Cr}-\text{Cr}$  distances of  $1.934(5)$  and  $2.644(5) \text{ \AA}$ , the degree of asymmetry approaching that observed in  $\text{Cr}_3(\text{dpa})_4(\text{X})(\text{Y})$  structures ( $\Delta d_{\text{Cr}-\text{Cr}} = 0.606 \text{ \AA}$ ,  $\text{X} = \text{Cl}$ ,  $\text{Y} = \text{PF}_6$ ,  $0.648 \text{ \AA}$ ,  $\text{X} = \text{Cl}$ ,  $\text{Y} = \text{BF}_4$ ), where the two terminal ligands are different. The dichloride-capped cation  $[\text{Cr}_3(\text{dpa})_4\text{Cl}_2]^+$  is also highly asymmetric ( $\Delta \text{Cr}-\text{Cr} = 0.431 \text{ \AA}$ ), as are all others containing the  $\text{Cr}_3^{7+}$  core.<sup>53</sup> The structure of the

NCS-capped  $\text{Cr}_5$  analogue,  $\text{Cr}_5(\text{tpda})_4(\text{NCS})_2$  ( $\text{tpda} = \text{tripyriddyldiamide}$ ), has been similarly controversial,<sup>54</sup> but disorder issues have been resolved to reveal a highly asymmetric  $\text{Cr}_5^{10+}$  core with alternating long and short bonds.<sup>55</sup> In their computational work, Bénard and Rohmer reported a perfectly symmetric equilibrium structure for  $\text{Cr}_3(\text{dpa})_4\text{Cl}_2$  with  $\text{Cr}-\text{Cr} = 2.35 \text{ \AA}$ , but also showed that distortion of the  $\text{Cr}_3$  chain is an energetically facile process, with even highly distorted structures ( $\Delta d_{\text{Cr}-\text{Cr}} = 0.679 \text{ \AA}$ ) lying only  $\sim 4 \text{ kcal/mol}$  higher in energy.<sup>39c,56</sup> Inspired by this structural diversity, Peng and co-workers proposed that the highly conducting "on" state observed in the CAFM experiments corresponds to a fully delocalized chain with four identical  $\text{Cr}-\text{Cr}$  bonds, while the "off" state features alternating long and short  $\text{Cr}-\text{Cr}$  bonds.<sup>44b</sup> Indeed, the idea that a symmetric (delocalized) structure is synonymous with efficient charge transport, and therefore that "breaks" in the delocalization will increase resistance, appears to be deeply embedded in the literature.<sup>35</sup> It is not clear, however, to what extent the long  $\text{Cr}-\text{Cr}$  bond in even the most unsymmetric structure is truly "broken", as even bond lengths of  $\sim 2.6 \text{ \AA}$  remain comfortably within the range of known metal-metal single bonds. Our purpose here is to establish a direct connection between electronic structure and electron transport by computing the zero-bias conductance from first principles.

In a recent paper,<sup>57</sup> we used density functional theory in conjunction with nonequilibrium Green's functions<sup>58,59</sup> to establish a direct link between the electron transport properties of the  $\text{Co}_3$  chain,  $\text{Co}_3(\text{dpa})_4(\text{NCS})_2$ , and its underlying electronic structure. We showed that the  $\text{Co}-\text{Co}-\text{Co}$   $\sigma^{\text{nb}}$  orbital lies closest to the Fermi level of the gold electrodes and is therefore the dominant conduction channel. In this work, we apply the same methodology to analyze the behavior of  $\text{Cr}_3(\text{dpa})_4(\text{NCS})_2$  and in particular to explore two closely connected hypotheses: (a) that the intrinsically higher conductance of the  $\text{Cr}_3$  chains is a direct result of the multiple bonding between the chromium centers and (b) that bimodal conductance profiles might arise in the chromium chains through switching between symmetric and unsymmetric forms. We conclude that the  $\pi$  bonding is largely irrelevant to the electron transport process, and that the  $\sigma$  framework is the dominant charge carrier, just as it is in the  $\text{Co}_3$  analogue. Low-symmetry distortions of the  $\text{Cr}_3$  core still influence the conductance by perturbing the 3-center-3-electron  $\sigma$  framework, but, rather counterintuitively, the conductance increases as the chain becomes more distorted.

## COMPUTATIONAL METHODS

All gas-phase calculations on  $\text{Cr}_3(\text{dpa})_4(\text{NCS})_2$  (quintet ground state) and  $\text{Co}_3(\text{dpa})_4(\text{NCS})_2$  (doublet ground state) were performed using the ADF2008<sup>60</sup> package and the PBE functional. A triple- $\zeta$  quality basis of Slater-type functions was used on the metals and double- $\zeta$  + polarization elsewhere. The spin-dependent electron transport properties were computed using the AtomisticToolkit software package, ATK2008.<sup>61,62</sup> The methodology combines a density functional theory treatment of the electronic structure with the Keldysh nonequilibrium Green's function approach to simulating coherent transport.<sup>63</sup> The scattering region,  $[\text{Au}_{32}]-\text{Cr}_3(\text{L})_4(\text{NCS})_2-[\text{Au}_{48}]$ , contains the EMAC, the geometry of which was taken from the fully or partially optimized gas-phase structure (computed with the ADF program as described above) and simplified as illustrated in Figure 1 (model ligand L). The relevant C-C and N-C bonds of the pyridyl rings were truncated, and the valences were capped with hydrogen atoms at 1.1 and 1.0  $\text{ \AA}$ ,

**Table 1. Bond Lengths, Spin Densities, and Conductances for the Scattering Regions Used in the Two-Probe Calculations ([Au<sub>32</sub>]-M<sub>3</sub>(L)<sub>4</sub>(NCS)<sub>2</sub>-[Au<sub>48</sub>])**

	gas phase (ADF)								
	bond lengths/Å		spin densities						
	Cr <sub>1</sub> -Cr <sub>2</sub>	Cr <sub>2</sub> -Cr <sub>3</sub>	Cr <sub>1</sub>	Cr <sub>2</sub>	Cr <sub>3</sub>	energy/kcal/mol			
<i>s</i> -Cr <sub>3</sub> (L) <sub>4</sub> (NCS) <sub>2</sub>	2.36	2.36	3.44	-2.91	3.44	0.0			
<i>u</i> -Cr <sub>3</sub> (L) <sub>4</sub> (NCS) <sub>2</sub> (0.25)	2.23(F) <sup>a</sup>	2.48(F)	3.20	-2.81	3.57	-0.1			
<i>u</i> -Cr <sub>3</sub> (L) <sub>4</sub> (NCS) <sub>2</sub> (0.71)	1.93(F)	2.64(F)	2.07	-1.83	3.71	+3.5			
	two-probe (ATK)								
	bond lengths/Å		spin densities			conductance (G/μS)			
	Cr <sub>1</sub> -Cr <sub>2</sub>	Cr <sub>2</sub> -Cr <sub>3</sub>	Cr <sub>1</sub>	Cr <sub>2</sub>	Cr <sub>3</sub>	G <sub>tot</sub>	G <sub>α</sub>	G <sub>β</sub>	
<i>s</i> -Cr <sub>3</sub> (L) <sub>4</sub> (NCS) <sub>2</sub>	2.36	2.36	2.84	-2.68	2.89	4.48	4.36	0.12	
<i>u</i> -Cr <sub>3</sub> (L) <sub>4</sub> (NCS) <sub>2</sub> (0.25)	2.23	2.48	2.63	-2.57	3.01	5.22	5.07	0.15	
<i>u</i> -Cr <sub>3</sub> (L) <sub>4</sub> (NCS) <sub>2</sub> (0.71)	1.93	2.64	1.20	-1.40	3.04	17.25	17.15	0.10	
Co <sub>3</sub> (L) <sub>4</sub> (NCS) <sub>2</sub>	2.32	2.32	0.00	0.00	0.00	0.72	0.36	0.36	

<sup>a</sup> Bond lengths marked "F" are fixed in the partial optimization.

respectively. Although truncating a ligand across an aromatic bond in this way is clearly not ideal, it is necessary to reduce the dimensions of the unit cell in the directions perpendicular to the transport direction. Our previous work suggests that this simplification does not perturb the equilibrium electronic structure of the isolated molecule to any significant extent.<sup>57</sup> The molecule is sandwiched between two and three  $4 \times 4$  layers of the Au (111) surface of the electrodes with the sulfur atoms of the two NCS ligands located in 3-fold hollow sites in the Au (111) surface with Au-S distances of 2.52 Å. The precise details of the contact geometry remain a significant issue in all transport calculations; the "hollow-site" geometry with a gold-sulfur distance of  $\sim 2.5$  Å (corresponding to a distance of  $\sim 1.9$  between the sulfur and the surface) adopted here has been established as the global minimum for many examples of sulfur coordination to Au (111)<sup>64</sup> and is used in the majority of comparative studies.<sup>65</sup> We have also considered alternative "on-top" and "tilted" geometries (details in the Supporting Information, Figures S1 and S2, respectively), and our key conclusions regarding the transport mechanism are robust to these changes. A full set of Cartesian coordinates for the two-probe system is provided in the Supporting Information.

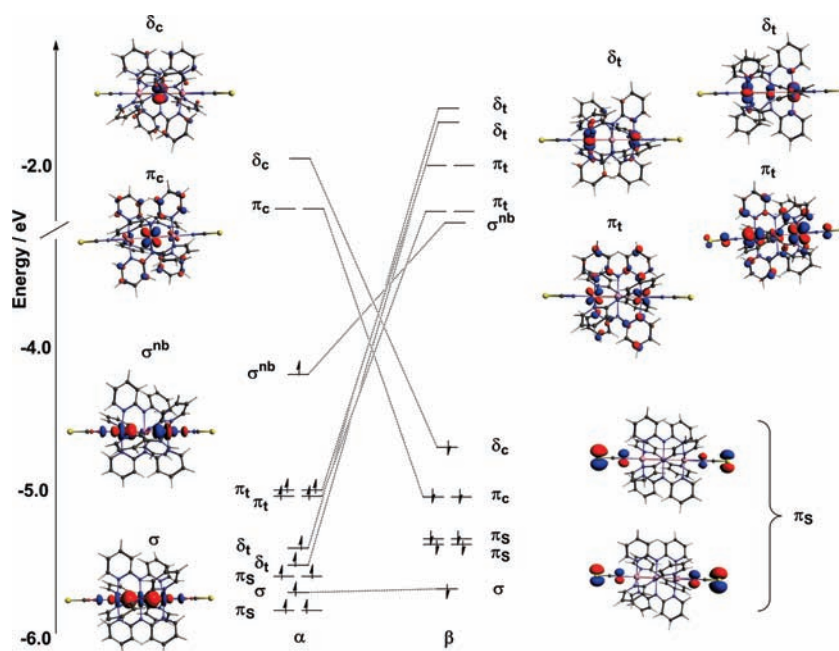
The transport calculations were performed using the LDA functional with the self-interaction correction (SIC) of Perdew and Zunger.<sup>66</sup> This choice of functional, and in particular the inclusion of the SIC, is motivated by the strongly correlated nature of the quintet ground state of Cr<sub>3</sub>(dpa)<sub>4</sub>(NCS)<sub>2</sub> (vide infra). The SIC has been shown to have a significant impact on transport calculations in exchange coupled systems, providing a better alignment of molecular levels with the Fermi level than alternative gradient corrected functional.<sup>27</sup> A parallel series of computations using the gradient-corrected PBE functional are presented and discussed in the Supporting Information (Figure S3). Numerical basis sets of single- $\zeta$  + polarization (SZP) quality on Au, double- $\zeta$  + polarization (DZP) on Cr, S, C, and H, and double- $\zeta$  + double polarization (DZDP) on nitrogen were used in all cases, and core electrons were described by norm-conserving pseudopotentials.<sup>67</sup> The initial spin density for the two-probe calculations was polarized to be consistent with the net spin densities of the isolated molecules in the gas phase. The electronic structure of the two-probe systems at equilibrium was converged using a 150 Ry mesh cutoff, a finite temperature of 300 K at the electrodes, and the real-space density constraint at the electrodes.

Sampling of the Brillouin zone was performed using a Monkhorst-Pack grid<sup>68</sup> with 300 *k*-points along the transport direction. The molecular orbitals in the scattering region are the eigenfunctions of the molecular projected self-consistent Hamiltonian (MPSH). At zero bias, the spin-dependent conductance,  $G_{\sigma}(0)$ , is given by the expression:

$$G_{\sigma}(0) = \left( \frac{dI}{dV} \right)_{V=0} = \frac{e^2}{h} T_{\sigma}(E_f, 0)$$

## RESULTS AND DISCUSSION

**Equilibrium Electronic Structure of Cr<sub>3</sub>(dpa)<sub>4</sub>(NCS)<sub>2</sub> in the Gas Phase.** As discussed in the Introduction, Bénard and Rohmer have analyzed in detail the electronic structure of Cr<sub>3</sub>(dpa)<sub>4</sub>Cl<sub>2</sub> in its quintet ground state.<sup>56</sup> Our focus is on the NCS-capped analogue, where the sulfur end groups ensure strong coupling to the gold electrode, but the basic features of the electronic structure prove to be essentially identical to those reported previously by the above authors. We therefore review only the key features that relate directly to the subsequent discussion of the electron transport properties. As was the case for the Cl-capped species, the quintet potential energy surface defined by the Cr-Cr-Cr asymmetric stretching mode is very flat. If the bond lengths are constrained to be equal, the optimized D<sub>4h</sub>-symmetric structure (denoted *s*-Cr<sub>3</sub>(dpa)<sub>4</sub>(NCS)<sub>2</sub> in Table 1) has Cr-Cr distances of 2.36 Å and net spin densities of +3.44 and -2.91 on the outer and inner chromium centers, respectively. These spin densities, along with an  $\langle S^2 \rangle$  value of 8.46 ( $\gg S(S+1) = 6.0$ ), are indicative of a highly localized broken-symmetry solution. The Kohn-Sham orbital spectrum for *s*-Cr<sub>3</sub>(dpa)<sub>4</sub>(NCS)<sub>2</sub> is summarized in Figure 2, where spin- $\alpha$  and spin- $\beta$  orbitals are shown as dashed blue and full red lines, respectively. The basic features are consistent with Bénard's previous analysis of Cr<sub>3</sub>(dpa)<sub>4</sub>Cl<sub>2</sub>, in so much as the spin polarization localizes the occupied spin- $\alpha$  orbitals on the terminal chromium centers ( $\pi_{\nu}$ ,  $\delta_{\nu}$ ) and their spin- $\beta$  counterparts on the central metal ( $\pi_{\sigma}$ ,  $\delta_{\sigma}$ ). Indeed, among the metal-based



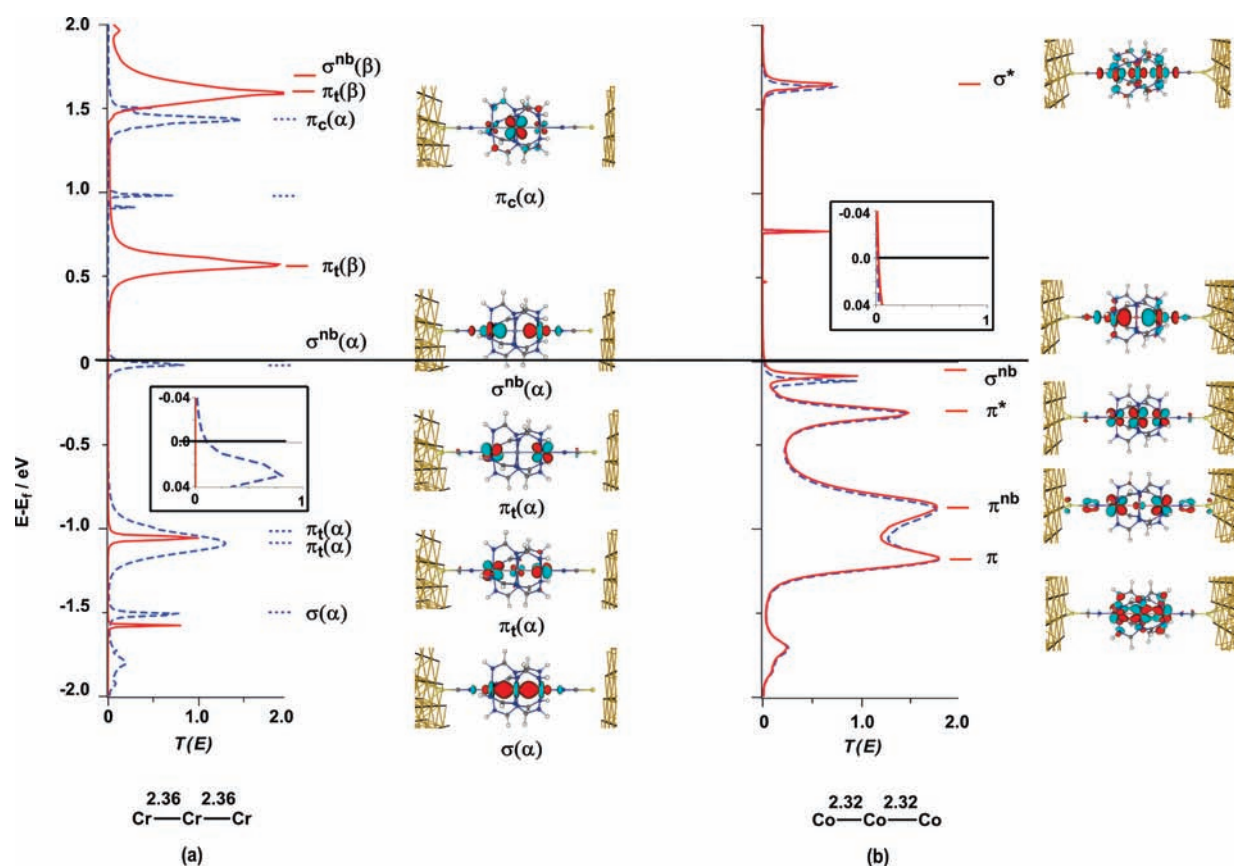
**Figure 2.** Frontier Kohn–Sham orbitals for *s*-Cr<sub>3</sub>(dpa)<sub>4</sub>(NCS)<sub>2</sub>. Dashed lines show correlations between orbitals with similar spatial properties in the spin- $\alpha$  and spin- $\beta$  manifolds.

orbitals, only the orbitals of  $\sigma$  symmetry show any significant delocalization over the entire Cr<sub>3</sub> unit. In addition to the metal-based  $\pi$  orbitals, a pair of sulfur-based orbitals of  $\pi$  symmetry ( $\pi_s$ ) is also present in the valence region. These mix extensively with their metal-based counterparts in the occupied spin- $\alpha$  manifold, where metal character is localized on the terminal chromiums, but not in the spin- $\beta$  set. The HOMO is the spin- $\alpha$  component of the  $\sigma^{nb}$  orbital, which is localized (by symmetry) on the terminal chromium centers. In short, the Cr–Cr–Cr interaction is dominated by a 3-center-3-electron  $\sigma$  bond,<sup>56</sup> just as it is in the cobalt analogue.<sup>42,57</sup>

In their original experimental work,<sup>44b</sup> Peng and co-workers proposed that the bimodal nature of the conductance histogram for the Cr<sub>5</sub> chains was caused by stochastic switching between structurally distinct “on” and “off” forms, and further that these “on” and “off” states corresponded to symmetric and unsymmetric forms of the chain, respectively. In support of this, Bénard and Rohmer’s DFT work indicates that while the equilibrium structure of Cr<sub>3</sub>(dpa)<sub>4</sub>Cl<sub>2</sub> is symmetric, distortion of the Cr<sub>3</sub> chain carries only a small energetic penalty, and our own calculations show that the same is true in the NCS-capped case. Thus, if the Cr–Cr distances are constrained at the values found for the crystal structure (2.23 and 2.48 Å, *u*-Cr<sub>3</sub>(dpa)<sub>4</sub>(NCS)<sub>2</sub> (0.25) in Table 1) and the remaining structural parameters optimized freely, the total energy is marginally (0.1 kcal/mol) lower than the symmetric structure. The difference of 0.1 kcal/mol is too small to interpret as significant, but it is nevertheless clear that the asymmetric stretch is very soft around the *D*<sub>4h</sub>-symmetric structure. Even for strongly distorted structures such as *u*-Cr<sub>3</sub>(dpa)<sub>4</sub>(NCS)<sub>2</sub> (0.71), where the Cr–Cr distances are constrained at the values found in the crystal structure of Cr<sub>3</sub>(dpa)<sub>4</sub>(NO<sub>3</sub>)<sub>2</sub> (1.93 and 2.64 Å), the system is destabilized by less than 4 kcal/mol (Table 1). The bonding in the unsymmetric form has been interpreted in terms of a shift toward a Cr≡Cr···Cr bonding pattern with a localized quadruple bond and a long nonbonded Cr···Cr contact.<sup>45</sup> The reduction in spin

densities at Cr<sub>1</sub> and Cr<sub>2</sub> in the unsymmetric form (Table 1) certainly indicates a greater degree of delocalization, but the spin densities remain  $\sim \pm 2.0$  even for very short Cr–Cr separations of 1.93 Å (Cr<sub>1</sub>–Cr<sub>2</sub>). Similarly, the spin density at the isolated Cr center is largely unaffected by increasing the Cr–Cr separation, even out to 2.64 Å, so it is not immediately obvious that this reaction coordinate really involves any substantial “breaking” of a bond. Instead, the facile distortion of the Cr<sub>3</sub> chain appears to be a result of the intrinsic flexibility of the 3-center-3-electron  $\sigma$  bond rather than any gross redistribution of the  $\pi/\delta$  framework. Whatever its underlying origins, the soft distortion mode of the Cr<sub>3</sub> chain means that external perturbations along the molecular *z* axis can distort the metal framework from its equilibrium geometry, a fact that is clearly reflected in the structural diversity of the Cr<sub>3</sub> cores.<sup>45</sup> In the context of this work, the applied potential provides just such a perturbation, and it is possible that the structure is therefore affected by bias. In the following discussion of electron transport, we take the range of Cr<sub>3</sub> core geometries known in the crystallographic database (i.e., completely symmetric,  $\Delta\text{Cr–Cr} = 0$ ; to grossly unsymmetric,  $\Delta\text{Cr–Cr} = 0.71$  Å) as a reasonable measure of the extent of distortion that might be induced by the electric field.

**Electron Transport.** The zero-bias transmission spectrum for the Cr<sub>3</sub>(L)<sub>4</sub>(NCS)<sub>2</sub> chain in its *D*<sub>4h</sub>-symmetric structure is shown in Figure 3a. The eigenstates of the molecular projected self-consistent Hamiltonian are also shown and can be compared to the Kohn–Sham orbitals of the isolated molecule shown in Figure 2. The region around the Fermi level is remarkably clean, with only a single narrow peak at  $E - E_f = -0.05$  eV with maximum  $T(E) \approx 1.0$  corresponding to the spin- $\alpha$  component of the  $\sigma^{nb}$  orbital. A similarly sharp peak centered on  $E - E_f = -1.5$  eV corresponds to the  $\sigma$  bonding orbital. A much broader feature with maximum  $T(E) > 1.0$  in the spin- $\alpha$  spectrum corresponding to the degenerate  $\pi$  orbitals on the outer chromium centers is located approximately 1.1 eV below the Fermi level. The extensive mixing of metal and sulfur-based orbitals



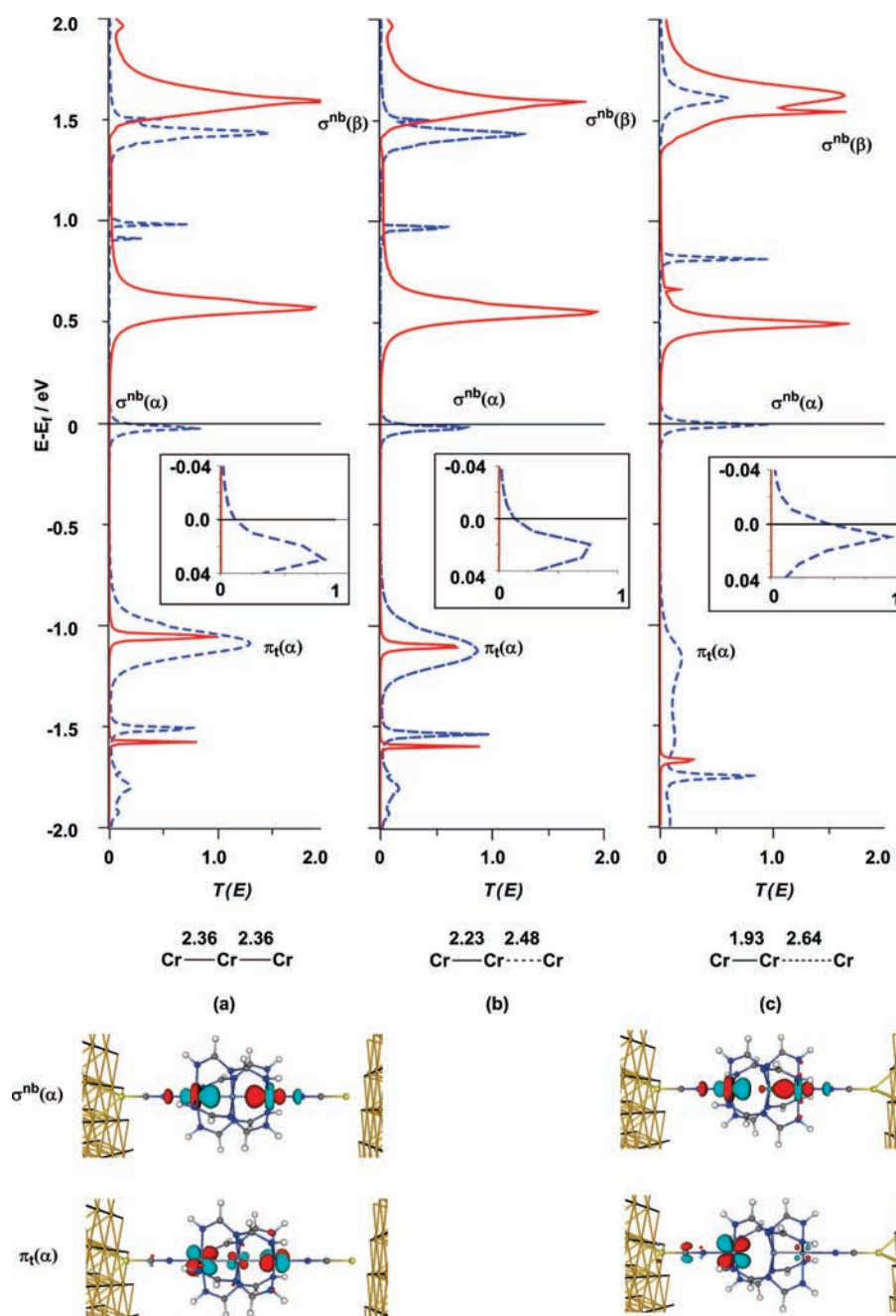
**Figure 3.** Spin- $\alpha$  (blue ---) and spin- $\beta$  (red —) transmission spectra for (a)  $s\text{-Cr}_3(\text{L})_4(\text{NCS})_2$  and (b)  $\text{Co}_3(\text{L})_4(\text{NCS})_2$ . Insets show magnifications of the region around the Fermi level.

of  $\pi$  symmetry that was apparent in the gas-phase calculations ensures strong coupling to the leads and therefore broadens these peaks in  $T(E)$ . The  $\pi$  orbitals in the spin- $\beta$  manifold (red line) appear in the same energetic window, but as they are localized on the central chromium atom they generate a much narrower feature in the transmission spectrum. The intensity of the spin- $\alpha$  resonances of  $\pi$  symmetry indicates that they are effective conduction channels, as anticipated by Peng and co-workers.<sup>44</sup> Their contribution to electron transport at moderate bias will nevertheless be negligible, simply because the relevant molecular levels are located far below  $E_F$ .

The computed values for the conductance are 4.48 and 0.72  $\mu\text{S}$  for  $\text{Cr}_3(\text{L})_4(\text{NCS})_2$  and  $\text{Co}_3(\text{L})_4(\text{NCS})_2$ , respectively (Table 1), and the ratio  $G(\text{Cr}_3)/G(\text{Co}_3)$  of 6.2 bisects the values determined from STM (2.1) and CAFM (17.6) experiments. The larger value for the chromium systems is, however, clearly not associated with any fundamental switch in the nature of the metal–metal bonding or indeed of the conduction pathway. The qualitative picture of the electron transport is remarkably insensitive to the identity of the metal: in both cases, the dominant channel is the  $\sigma^{\text{nb}}$  orbital localized on the outer metal centers, and the higher conductance of  $\text{Cr}_3(\text{L})_4(\text{NCS})_2$  arises simply because this channel lies closer to the Fermi level (compare Figure 3a and b).<sup>57</sup> The transmission spectra reveal a much higher degree of spin polarization in the  $\text{Cr}_3$  case, where the ground state of the isolated molecule is a quintet, as compared to the  $\text{Co}_3$  analogue, which is a doublet. Binding to the two gold electrodes does not substantially affect the spin densities on the

chromium centers, and as a result the zero-bias conductance is 99% spin polarized (spin- $\alpha$  dominant). In the cobalt case, in contrast, contact with the infinite gold reservoirs equalizes the spin densities on the cobalt centers, the result being much less strongly polarized current.<sup>69</sup>

The precise structure of the contact between molecule and electrode in the experimental measurements is, of course, unknown, and the large scatter in the experimental data<sup>44</sup> suggests that several geometries may be adopted. Our choice of 3-fold hollow sites in the Au(111) surface for both sulfur atoms is based on literature precedent; this geometry has been demonstrated to be the most stable in many sulfur-capped molecules and is commonly adopted in transport studies. There are, however, a number of alternatives, including geometries where the sulfur atoms sit either above a single atom (“on-top”) or above an edge. Asymmetric geometries where only one end of the molecule is placed in an “on-top” site while the other sits in a 3-fold hollow represent plausible models for the structure in STM break-junction experiments.<sup>70</sup> Moreover, it is possible that the molecule lies at an angle to the electrode surfaces, rather than normal to them as shown in Figure 1. Given the uncertainties in the experimental geometries, we have explored the impact of variations in the contact geometry on the conclusions set out in the previous paragraph. Specifically, we have used the “hollow/on-top” model for the break junction structure and also one where the molecule is tilted by  $\sim 20^\circ$  relative to the surface, such that the sulfur atoms sit in 3-fold hollows that are offset relative to each other. The transmission spectra shown in Figures S1 and S2



**Figure 4.** Transmission spectra for (a)  $s\text{-Cr}_3(\text{L})_4(\text{NCS})_2$ , (b)  $u\text{-Cr}_3(\text{L})_4(\text{NCS})_2$  (0.25), and (c)  $u\text{-Cr}_3(\text{L})_4(\text{NCS})_2$  (0.71). Contour plots of  $\sigma^{\text{nb}}$  and  $\pi_t$  eigenfunctions of the molecular projected self-consistent Hamiltonian are shown below for  $s\text{-Cr}_3(\text{L})_4(\text{NCS})_2$  and  $u\text{-Cr}_3(\text{L})_4(\text{NCS})_2$  (0.71).

confirm that the qualitative picture set out in the previous paragraphs is not significantly influenced by the contact geometry: in all cases, the  $\sigma^{\text{nb}}$  channel lies close to  $E_f$  and remains the dominant electron transport pathway. The insensitivity of the conductance to contact geometry arises because the orbitals that establish the coupling of the molecule to the electrode (the  $\pi$  orbitals localized on the sulfur) are strictly orthogonal to the dominant transport channel (the Cr-based  $\sigma^{\text{nb}}$  orbital).

We now explore the influence of structural distortions on the conductance of the  $\text{Cr}_3$  chain, and in particular the hypothesis that such distortions might reduce the conductance, yielding an “off” state in a putative molecular switch. In the discussion of the structural chemistry, we highlighted the fact that, depending on

the terminal ligands, the  $\text{Cr}_3$  core can be totally symmetric ( $X = \text{CN}^-$ ,  $\text{CCPh}^-$ ), marginally distorted as in the crystal structure for  $X = \text{NCS}^-$  itself ( $\text{Cr}-\text{Cr} = 2.23$  and  $2.48$  Å), or even highly distorted as in the  $\text{NO}_3^-$ -capped species (1.93 and 2.64 Å).<sup>45</sup> Accordingly, we have recomputed the transmission spectrum and conductance of  $\text{Cr}_3(\text{L})_4(\text{NCS})_2$  for cases where the  $\text{Cr}_3$  core is distorted, both marginally (2.23, 2.48; Figure 4b) and strongly (1.93, 2.64; Figure 4c). The geometries of the scattering region were taken from the partially optimized structures  $u\text{-Cr}_3(\text{L})_4(\text{NCS})_2$  (0.25) and  $u\text{-Cr}_3(\text{L})_4(\text{NCS})_2$  (0.71) discussed above, truncated as before by removing the bulk of the aromatic ligand capping dangling valences with hydrogens. The same contact geometry used for the symmetric case was retained, that is, sulfur

in a hollow site with Au–S = 2.52 Å. Around the Fermi level, the transmission spectra for the distorted structures (Figure 4b,c) are qualitatively very similar to that for the symmetric form (Figure 4a), with an intense peak corresponding to the spin- $\alpha$   $\sigma^{\text{nb}}$  channel lying very close to  $E_{\text{f}}$ . As the structure becomes more distorted, the intense spin- $\alpha$  peaks in the region of  $E - E_{\text{f}} = -1.1$  eV for the  $\pi_{\text{t}}$  channel become progressively broader and less intense, to the point where the peak transmission is <0.2 for the most highly distorted structure. The eigenfunctions of the molecular projected self-consistent Hamiltonian indicate the origin of this effect: the structural asymmetry induces substantial mixing of the near degenerate in- and out-of-phase combinations of the  $\pi_{\text{t}}$  orbitals. This in turn localizes the orbitals on one side or other of the molecule and effectively closes off the  $\pi$  channels. We have previously noted similar features for the cobalt complex under applied bias, where the electric field, rather than any intrinsic geometric asymmetry, was responsible for the closure of the  $\pi$  channels.<sup>57</sup> Thus, the simple expectation that structural asymmetry should reduce transport through the  $\pi$  channels is valid, but this has negligible impact on the low-bias conductance, simply because the levels in question lie so far below the Fermi level. The most significant change induced by the distortion is in fact rather more subtle: the dominant  $\sigma$  channel is shifted upward toward  $E_{\text{f}}$ , albeit only marginally, leading to an approximate 4-fold increase in conductance (4.48 vs 17.25  $\mu\text{S}$ ) in the limit of extreme distortion (the insets again magnify the changes around the Fermi level). The upward shift in the  $\sigma^{\text{nb}}$  level can be traced to a rehybridization within the  $\sigma/\sigma^{\text{nb}}/\sigma^*$  framework, which causes the  $\sigma^{\text{nb}}$  orbital to develop some antibonding character with respect to the central chromium  $d_{z^2}$  orbital. The rehybridization is much less pronounced than in the  $\pi$  manifold, simply because the first-order separation of the  $\sigma$ ,  $\sigma^{\text{nb}}$ , and  $\sigma^*$  orbitals is much greater. Nevertheless, the distortion of the  $\text{Cr}_3$  chain results, perhaps counterintuitively, in greater delocalization of the key transmission channel.

It is important to acknowledge that the computed conductance depends only on the transmission coefficient at one specific energy, the Fermi level, and the ability of DFT to accurately place the molecular levels relative to this reference point is therefore critical. We believe, however, that our conclusions regarding the impact of asymmetry on the conductance of the  $\text{Cr}_3$  chains are robust for two reasons. First, our focus on the  $\sigma^{\text{nb}}$  channel is justified because the window around the Fermi level is very clean, and an upward shift of almost 1 eV in the molecular levels would be required before the  $\pi$  channels became significant. Second, the key destabilization of the  $\sigma^{\text{nb}}$  orbital upon distortion is an intrinsic property of the molecule that is also apparent in the gas-phase calculations. Moreover, it correlates with the experimental observation that the cationic  $[\text{Cr}_3(\text{dpa})_4\text{X}_2]^+$  species, where this orbital is indisputably vacant, all adopt highly unsymmetric structures. Thus, so long as the occupied spin- $\alpha$  component of the  $\sigma^{\text{nb}}$  orbital lies below the Fermi level in the symmetric system (i.e., the molecule is not oxidized upon binding to the gold electrode), any distortion must necessarily lead to enhanced conductance as this orbital is driven upward.

In summary, our computational analysis suggests that low-symmetry distortions of the  $\text{Cr}_3(\text{dpa})_4(\text{NCS})_2$  chain serve to enhance, rather than disrupt, its ability to transport electrons. The  $\pi$  orbitals are largely irrelevant in this regard as they are strongly stabilized and lie >1 eV below the Fermi level. Instead, the dominant pathway is through the nonbonding combination of  $d_{z^2}$  orbitals, which is entirely localized on the terminal

chromium centers in the symmetric case. Distortions away from strict  $D_4$  symmetry allow mixing of the  $\sigma$ ,  $\sigma^{\text{nb}}$ , and  $\sigma^*$  levels and introduce a small amount of  $d_{z^2}$  character from the central chromium into this orbital. The result is that it is displaced upward toward the Fermi level, enhancing the computed conductance. While the increase is marginal, it is very clear that there is absolutely no evidence to suggest that the distortion should diminish the flow of current through the system, as has been proposed for the related  $\text{Cr}_5$  chains. In more general terms, the density of states around the Fermi level in a chain of transition metal ions is complex, and the rational design of molecular conductors based on these architectures requires a detailed consideration of the electronic structure.

## ■ ASSOCIATED CONTENT

**S Supporting Information.** Transmission spectra for “on-top” (Figure S1) and “tilted” (Figure S2) geometries, and also for calculations performed with the PBE functional (Figure S3). Total energies and Cartesian coordinates for all optimized structures and also for all scattering regions in the two-probe calculations. Complete ref 60. This material is available free of charge via the Internet at <http://pubs.acs.org>.

## ■ AUTHOR INFORMATION

### Corresponding Author

[john.mcgrady@chem.ox.ac.uk](mailto:john.mcgrady@chem.ox.ac.uk)

## ■ ACKNOWLEDGMENT

We acknowledge the EPSRC (EP/F019327/1) for financial support and the Oxford Supercomputer Center (OSC) for computational resources.

## ■ REFERENCES

- (1) Aviram, A.; Ratner, M. *Chem. Phys. Lett.* **1974**, *29*, 277.
- (2) (a) Moore, G. E. *Electronics* **1965**, *38*, 114. (b) Reed, M. A.; Tour, J. *Sci. Am.* **2000**, *282*, 86. (c) Nitzan, A.; Ratner, M. A. *Science* **2003**, *300*, 1384.
- (3) (a) Kim, W. Y.; Kim, K. S. *Acc. Chem. Res.* **2010**, *43*, 111. (b) Xue, Y.; Ratner, M. A. *Phys. Rev. B* **2004**, *69*, 085403. (c) Xue, Y.; Ratner, M. A. *Phys. Rev. B* **2003**, *68*, 115406. (d) Gonzalez, C.; Simón-Manso, Y.; Batteas, J.; Marquez, M.; Ratner, M. A.; Mujica, V. *J. Phys. Chem. B* **2004**, *108*, 18414. (e) Mujica, V.; Roitberg, A. E.; Ratner, M. A. *J. Chem. Phys.* **2000**, *112*, 6834. (f) Liang, G. C.; Ghosh, A. W.; Paulsson, M.; Datta, S. *Phys. Rev. B* **2004**, *69*, 115302.
- (4) (a) Chappert, C.; Fert, A.; Van Dau, F. N. *Nat. Mater.* **2007**, *6*, 812. (b) Sanvito, S. *Nat. Mater.* **2007**, *6*, 804. *Nat. Nanotechnol.* **2007**, *264*. (c) Sulczewski, G.; Sanvito, S.; Corey, M. *Nat. Mater.* **2009**, *693*. (d) Camarero, J.; Coronado, E. *J. Mater. Chem.* **2009**, *19*, 1678. (e) Bibes, M.; Barthelemy, A. *Nat. Mater.* **2008**, *7*, 425.
- (5) Pontes, R. B.; da Silva, E. Z.; Fazzio, A.; da Silva, A. J. R. *J. Am. Chem. Soc.* **2008**, *130*, 9897.
- (6) Tao, K.; Rungger, I.; Sanvito, S.; Stepanyuk, V. S. *Phys. Rev. B* **2010**, *82*, 085412.
- (7) Liu, R.; Ke, S.-H.; Yang, W.; Baranger, H. U. *J. Chem. Phys.* **2007**, *127*, 141104.
- (8) (a) Li, Y. W.; Yao, J. H.; Liu, C. J.; Yang, J. W.; Yang, C. L. *Phys. Lett. A* **2009**, *373*, 3974. (b) Yao, J. H.; Deng, X. S.; Yang, C. L. *Phys. E (Amsterdam, Neth.)* **2010**, *43*, 382. (c) Liu, H.; Xu, Z.; Wang, N.; Yu, C.; Gao, N.; Zhao, J.; Li, N. *J. Chem. Phys.* **2010**, *132*, 244702. (d) Nan, W.; Liu, H.; Zhao, J.; Cui, Y.; Xu, Z.; Ye, Y.; Kiguchi, M.; Murakoshi, K. *J. Phys. Chem. C* **2009**, *113*, 7416.



- (9) (a) Xin, S.; Sun, L.; Yi, Z.; Benassi, E.; Zhang, R.; Shen, Z.; Sanvito, S.; Hou, S. *Phys. Chem. Chem. Phys.* **2010**, *12*, 10805. (b) Tada, T.; Hamayama, S.; Kondo, M.; Yoshizawa, K. *J. Phys. Chem. B* **2005**, *109*, 12443. (c) Calzolari, A.; Ferretti, A.; Nardelli, M. B. *Nanotechnology* **2007**, *18*, 424013. (d) Shen, X.; Sun, L.; Benassi, E.; Shen, Z.; Zhao, X.; Sanvito, S.; Hou, S. *J. Chem. Phys.* **2010**, *132*, 054703.
- (10) (a) Das, B. *J. Phys. Chem. C* **2009**, *113*, 16203. (b) Das, B.; Abe, S. *J. Phys. Chem. B* **2006**, *110*, 23806.
- (11) Sen, S.; Chakrabarti, S. *J. Am. Chem. Soc.* **2010**, *132*, 15334.
- (12) (a) Wang, L.; Cai, Z.; Wang, J.; Lu, J.; Luo, G.; Lai, L.; Zhou, J.; Qin, R.; Gao, Z.; Yu, D.; Li, G.; Mei, W. N.; Sanvito, S. *Nano Lett.* **2008**, *8*, 3640. (b) Garcia-Suarez, V.; Jaime Ferrer, J.; Lambert, C. *J. Phys. Rev. Lett.* **2006**, *96*, 106804. (c) Yi, Z.; Shen, X.; Sun, L.; Shen, Z.; Hou, S.; Sanvito, S. *ACS Nano* **2010**, *4*, 2274.
- (13) (a) Wu, J.-C.; Wang, X.-F.; Zhou, L.; Da, H.-X.; Lim, K. H.; Yang, S.-W.; Li, Z.-Y. *J. Phys. Chem. C* **2009**, *113*, 7913. (b) Zhou, L.; Yang, S.-Y.; Ng, M.-F.; Sullivan, M. B.; Tan, V. B. C.; Shen, L. *J. Am. Chem. Soc.* **2008**, *130*, 4023.
- (14) Zhang, G.; Qin, Y.; Zhang, H.; Shang, Y.; Sun, M.; Liu, B.; Li, Z. *J. Phys. Chem. C* **2010**, *114*, 9469.
- (15) (a) Maslyuk, V. V.; Bagrets, A.; Meded, V.; Arnold, A.; Evers, F.; Brandbyge, M.; Bredow, T.; Mertig, I. *Phys. Rev. Lett.* **2006**, *97*, 097201. (b) Koleini, M.; Paulsson, M.; Brandbyge, M. *Phys. Rev. Lett.* **2007**, *98*, 197202. (c) Xiang, H.; Yang, J.; Hou, J. G.; Zhu, Q. *J. Am. Chem. Soc.* **2006**, *128*, 2310. (d) Hou, S.; Chen, Y.; Shen, X.; Li, R.; Ning, J.; Qian, Z.; Sanvito, S. *Chem. Phys.* **2008**, *354*, 106.
- (16) (a) Mallajosyula, S. S.; Parida, P.; Pati, S. K. *J. Mater. Chem.* **2009**, *19*, 1761. (b) Zhu, L.; Wang, J. *J. Phys. Chem. C* **2009**, *113*, 8767.
- (17) Kang, H. S. *J. Phys. Chem.* **2010**, *114*, 11266.
- (18) Xu, K.; Huang, J.; Lei, S.; Su, H.; Boey, F. Y. C.; Li, Q.; Yang, J. *J. Chem. Phys.* **2009**, *131*, 104704. (b) Huang, J.; Li, Q.; Xu, K.; Su, H.; Yang, J. *J. Phys. Chem. C* **2010**, *114*, 11946.
- (19) (a) Liu, R.; Ke, S.-H.; Baranger, H. U.; Yang, W. *Nano Lett.* **2005**, *5*, 1959. (b) Baadji, N.; Piacenze, M.; Tugsuz, T.; Sala, F. D.; Maruccio, G.; Sanvito, S. *Nat. Mater.* **2009**, *8*, 813.
- (20) Ulises Reveles, J.; Clayborne, P. A.; Reber, A. C.; Khanna, S. N.; Pradhan, K.; Sen, P.; Pederson, M. R. *Nat. Chem.* **2009**, *1*, 310.
- (21) He, H.; Pandey, R.; Reveles, J. U.; Khanna, S. N.; Karna, S. P. *Appl. Phys. Lett.* **2009**, *95*, 192104.
- (22) Hao, H.; Xheng, X. H.; Dai, Z. X.; Zeng, Z. *App. Phys. Lett.* **2010**, *96*, 192112.
- (23) Zhu, L.; Yao, K. L.; Liu, Z. L. *App. Phys. Lett.* **2010**, *96*, 082115.
- (24) (a) Heersche, H. B.; de Groot, Z.; Folk, J. A.; van der Zant, H. S.; Romeike, C.; Wegewijs, M. R.; Zobbi, L.; Barreca, D.; Tondello, E.; Cornia, A. *Phys. Rev. Lett.* **2006**, *96*, 206801. (b) Jo, M.-H.; Grose, J. E.; Baheti, K.; Deshmukh, M. M.; Sokol, J. J.; Rumberger, E. M.; Hendrickson, D. N.; Long, J. R.; Park, H.; Ralph, D. C. *Nano Lett.* **2006**, *6*, 2014.
- (25) Barraza-Lopez, S.; Park, K.; Garcia-Suarez, V.; Ferrer, J. *J. Appl. Phys.* **2009**, *105*, E7E309.
- (26) Boani, L.; Wernsdorfer, W. *Nat. Mater.* **2008**, *7*, 179.
- (27) Pemmeraju, C. D.; Rungger, I.; Sanvito, S. *Phys. Rev. B* **2009**, *80*, 104422.
- (28) (a) Senger, R. T.; Tongay, S.; Durgun, E.; Ciraci, S. *Phys. Rev. B* **2005**, *72*, 075419. (b) Garcia-Suarez, V. M.; Manrique, D. Z.; Lambert, C. J.; Ferrer, J. *Phys. Rev. B* **2009**, *79*, 060408(R). (c) Garcia-Suarez, V.; Reily Rocha, A.; Bailey, S. W.; Lambert, C. J.; Sanvito, S.; Ferrer, J. *Phys. Rev. Lett.* **2005**, *95*, 256804. (d) Garcia-Fuente, A.; Vega, A.; Garcia-Suarez, V. M.; Ferrer, J. *Nanotechnology* **2010**, *21*, 095205. (e) Xu, Y.; Shi, X.; Zeng, Z.; Zenf, Z. Y.; Li, B. *J. Phys.: Condens. Matter* **2007**, *19*, 056010.
- (29) (a) Min, Y.; Yao, K. L.; Liu, Z. L.; Gao, G. Y.; Cheng, H. G.; Zhu, S. C. *Nanotechnology* **2009**, *20*, 095201. (b) Yang, C. K.; Zhao, J.; Lu, J. P. *Phys. Rev. Lett.* **2003**, *90*, 257203. (c) Jo, C. *J. Phys. D* **2009**, *42*, 105008. (d) Jo, C.; Il Lee, J. *J. Magn. Magn. Mater.* **2008**, *320*, 3256. (e) Jang, Y. R.; Lee, J. I. *Phys. Status Solidi B* **2007**, *244*, 4407. (f) Ivanovskaya, V. V.; Kohler, C.; Seifert, G. *Phys. Rev. B* **2007**, *75*, 075410. (g) Jo, C. L.; Lee, J. I.; Jang, Y. R. *Phys. Status Solidi C* **2004**, *3264*. (h) Parq, J. H.; Yu, J.; Kim, G. *J. Chem. Phys.* **2010**, *132*, 054701.
- (30) Yang, T.; Berber, S.; Tomanek, D. *Phys. Rev. B* **2008**, *77*, 165426.
- (31) Nguyen, T.; Sutton, A. D.; Brynda, M.; Fettinger, J. C.; Long, G. J.; Power, P. P. *Science* **2005**, *310*, 844.
- (32) (a) Kreisel, K. A.; Yap, G. P. A.; Dmitrenko, O.; Landis, C. R.; Theopold, K. H. *J. Am. Chem. Soc.* **2007**, *129*, 14162. (b) Noor, A.; Wagner, F. R.; Kempe, R. *Angew. Chem., Int. Ed.* **2008**, *47*, 7246.
- (33) Huang, J.; Li, Q.; Ren, H.; Su, H.; Yang, J. *J. Chem. Phys.* **2006**, *125*, 184713.
- (34) (a) Yeh, C.-Y.; Wang, C.-C.; Chen, C.-H.; Peng, S.-M. In *Redox Systems Under Nano-Space Control*; Hirao, T., Ed.; Springer: Berlin, 2006. (b) Liu, I. P.-C.; Wang, W.-Z.; Peng, S.-M. *Chem. Commun.* **2009**, 4323. (c) Cheng, C.-H.; Hung, R.-D.; Wang, W.-Z.; Peng, S.-M.; Chia, C.-I. *ChemPhysChem* **2010**, *11*, 466.
- (35) Berry, J. F. In *Multiple Bonds Between Metal Atoms*; Cotton, F. A.; Murillo, C. A.; Walton, R. A., Eds.; Springer: New York, 2005. (b) Berry, J. F. *Struct. Bonding (Berlin)* **2010**, *136*, 1.
- (36) Cotton, F. A. *Inorg. Chem.* **1998**, *37*, 5710.
- (37) Ismailov, R.; Weng, W.-Z.; Wang, R.-R.; Huang, Y.-L.; Yeh, C.-Y.; Lee, G.-H.; Peng, S.-M. *Eur. J. Inorg. Chem.* **2008**, 4290.
- (38) (a) Yang, E.-C.; Cheng, M.-C.; Tsai, M.-S.; Peng, S.-M. *J. Chem. Soc., Chem. Commun.* **1994**, 2377. (b) Clérac, R.; Cotton, F. A.; Daniels, L. M.; Dunbar, K. R.; Kirschbaum, K.; Murillo, C. A.; Pinkerton, A. A.; Schultz, A. J.; Wang, X. *J. Am. Chem. Soc.* **2000**, *122*, 6226. (c) Clérac, R.; Cotton, F. A.; Daniels, L. M.; Dunbar, K. R.; Murillo, C. A.; Wang, X. *Inorg. Chem.* **2001**, *40*, 1256.
- (39) (a) Yang, E.-C.; Cheng, M.-C.; Tsai, M.-S.; Peng, S.-M. *J. Chem. Soc., Chem. Commun.* **1994**, 2377. (b) Clérac, R.; Cotton, F. A.; Daniels, L. M.; Dunbar, K. R.; Kirschbaum, K.; Murillo, C. A.; Pinkerton, A. A.; Schultz, A. J.; Wang, X. *J. Am. Chem. Soc.* **2000**, *122*, 6226. (c) Clérac, R.; Cotton, F. A.; Daniels, L. M.; Dunbar, K. R.; Murillo, C. A.; Wang, X. *Inorg. Chem.* **2001**, *40*, 1256.
- (40) (a) Rohmer, M.-M.; Bénard, M. *J. Am. Chem. Soc.* **1998**, *120*, 9372. (b) Rohmer, M.-M.; Strich, A.; Bénard, M.; Malrieu, J.-P. *J. Am. Chem. Soc.* **2001**, *123*, 9126. (c) Rohmer, M.-M.; Bénard, M. *Chem. Soc. Rev.* **2001**, *30*, 340.
- (41) Poulsen, R. D.; Overgaard, J.; Schulman, A.; Østergaard, C.; Murillo, C. A.; Spackman, M. A.; Iversen, B. B. *J. Am. Chem. Soc.* **2009**, *131*, 7580.
- (42) (a) Pantazis, D. A.; McGrady, J. E. *J. Am. Chem. Soc.* **2006**, *128*, 4128. (b) Pantazis, D. A.; Murillo, C. A.; McGrady, J. E. *Dalton Trans.* **2008**, 608. (c) McGrady, J. E.; Pantazis, D. A. *Chemtracts: Inorg. Chem.* **2005**, *18*, 629.
- (43) Berry, J. F.; Cotton, F. A.; Daniels, L. M.; Murillo, C. M.; Wang, X. *Inorg. Chem.* **2003**, *42*, 2418.
- (44) (a) Lin, S.-Y.; Chen, I.-W. P.; Chen, C.-h.; Hsieh, M.-H.; Yeh, C.-Y.; Lin, T.-W.; Chen, Y.-H.; Peng, S.-M. *J. Phys. Chem. B* **2004**, *108*, 959. (b) Chen, I.-W. P.; Fu, M.-D.; Tseng, W.-H.; You, J.-Y.; Wu, S.-H.; Ku, C.-J.; Chen, C.-h.; Peng, S.-M. *Angew. Chem., Int. Ed.* **2006**, *45*, 5814. (c) Shin, K.-N.; Huang, M.-J.; Lu, H.-G.; Fu, M.-D.; Kuo, C.-K.; Huang, G.-C.; Lee, G.-H.; Chen, C.-h.; Peng, S.-M. *Chem. Commun.* **2010**, 46, 1338.
- (45) Berry, J. F.; Cotton, F. A.; Lu, T.; Murillo, C. A.; Roberts, B. K.; Wang, X. *J. Am. Chem. Soc.* **2004**, *126*, 7082.
- (46) Chae, D.-H.; Berry, J. F.; Jung, S.; Cotton, F. A.; Murillo, C. A.; Yao, Z. *Nano Lett.* **2006**, *6*, 165.
- (47) Kiehl, P.; Rohmer, M.-M.; Bénard, M. *Inorg. Chem.* **2004**, *43*, 3151.
- (48) Paul, F.; Lapinte, C. *Coord. Chem. Rev.* **1998**, *178–180*, 431.
- (49) (a) Hsu, L. Y.; Huang, Q. R.; Jin, B.-Y. *J. Phys. Chem. C* **2008**, *112*, 10538. (b) Tsai, T. W.; Huang, Q.-R.; Peng, S.-M.; Jin, B.-Y. *J. Phys. Chem. C* **2010**, *114*, 3641.
- (50) Clerac, R.; Cotton, F. A.; Daniels, L. M.; Dunbar, K. R.; Murillo, C. A.; Pascual, I. *Inorg. Chem.* **2000**, *39*, 748.
- (51) Hsiao, C.-J.; Lai, S.-H.; Chen, I.-C.; Wang, W.-Z.; Peng, S.-M. *J. Phys. Chem. A* **2008**, *112*, 13528.
- (52) Lin, S.-Y.; Chen, I.-W.; Chen, C.-h.; Hsieh, M.-H.; Yeh, C. -Y.; Lin, T.-W.; Chen, Y.-H.; Peng, S.-M. *J. Phys. Chem. B* **2004**, *108*, 959.

- (53) Clerac, R.; Cotton, F. A.; Daniels, L. M.; Dunbar, K. R.; Murillo, C. A.; Pascual, I. *Inorg. Chem.* **2000**, *39*, 752.
- (54) Chang, H.-C.; Li, J.-T.; Wang, C.-C.; Lin, T.-W.; Lee, H.-C.; Lee, G.-H.; Peng, S.-M. *Eur. J. Inorg. Chem.* **1999**, 1243.
- (55) Berry, J. F.; Cotton, F. A.; Fewox, C. S.; Lu, T.; Murillo, C. A.; Wang, X. *Dalton Trans.* **2004**, 2297.
- (56) (a) Benbellat, N.; Rohmer, M.-M.; Bénard, M. *Chem. Commun.* **2001**, 2368. (b) Rohmer, M.-M.; Bénard, M. *J. Cluster Sci.* **2002**, *13*, 333.
- (57) Georgiev, V. P.; McGrady, J. E. *Inorg. Chem.* **2010**, *49*, 5591.
- (58) (a) Kim, W. Y.; Choi, Y. C.; Min, S. K.; Cho, Y.; Kim, K. S. *Chem. Soc. Rev.* **2009**, *38*, 2319. (b) Koentopp, M.; Chang, C.; Burke, K.; Car, R. *J. Phys.: Condens. Matter* **2008**, *20*, 083203.
- (59) Paulsson, M. Non-equilibrium Green's Functions for Dummies; <http://www.nanohub.org/resources/1932>.
- (60) Baerends, E. J.; et al.
- (61) <http://www.quantumwise.com/>.
- (62) (a) Brandbyge, M.; Mozos, J.-L.; Ordejon, P.; Taylor, P.; Stokbro, K. *Phys. Rev. B* **2002**, *65*, 165401. (b) Soler, J. M.; Artacho, E.; Gale, J. D.; Garcia, A.; Unquera, J.; Ordejon, P.; Sanchez-Portal, D. *J. Phys.: Condens. Matter* **2002**, *14*, 2745. (c) Taylor, J.; Guo, H.; Wang, J. *Phys. Rev. B* **2001**, *63*, 245407.
- (63) (a) Datta, S. *Electron Transport in Mesoscopic Systems*; Cambridge University Press: Cambridge, UK, 1997. (b) Datta, S. *Quantum Transport: Atom to Transistor*; Cambridge University Press: Cambridge, UK, 2005. (c) Jortner, J.; Nitzan, A.; Ratner, M. A. *Lecture Notes in Physics, Introducing Molecular Electronics*; Springer: New York, 2005, 14. (d) Lindsay, S. *Faraday Discuss.* **2006**, *131*, 403. (e) Smit, R. H.; Noat, Y.; Untiedt, C.; Lang, N. D.; van Hemert, M. C.; van Ruitenbeek, J. M. *Nature* **2002**, *419*, 906. (f) Yu, L. H.; Keane, Z. K.; Ciszek, J. W.; Cheng, L.; Stewart, M. P.; Tour, J. M.; Natelson, D. *Phys. Rev. Lett.* **2004**, *93*, 266802.
- (64) Toher, C.; Sanvito, S. *Phys. Rev. B* **2008**, *77*, 155402.
- (65) (a) Cohen, R.; Stokbro, K.; Martin, J. M. L.; Ratner, M. A. *J. Phys. Chem. C* **2007**, *111*, 14893. (b) Liu, H.; Yu, C.; Gao, N.; Zhao, J. *ChemPhysChem* **2010**, *11*, 1895. (c) Tagami, K.; Tsukuda, M. *J. Phys. Chem. B* **2004**, *108*, 6441.
- (66) Perdew, J. P.; Zunger, A. *Phys. Rev. B* **1981**, *23*, 5048.
- (67) Troullier, N.; Martins, J. L. *Phys. Rev. B* **1991**, *43*, 1993.
- (68) Monkhorst, H. J.; Pack, J. D. *Phys. Rev. B* **1976**, *13*, 5188.
- (69) In our previous work in ref 57 performed with the PBE functional, we reported a much higher degree of spin polarization in the Co<sub>3</sub> case.
- (70) (a) Sheng, W.; Li, Z. Y.; Ning, Z. Y.; Zhang, Z. H.; Yang, Z. Q.; Guo, H. *J. Chem. Phys.* **2009**, *131*, 244712. (b) Wang, C.; Batsanov, A. S.; Bryce, M. R.; Martin, S.; Nichols, R. J.; Higgins, S. J.; Garcia-Suarez, V. M.; Lambert, C. J. *J. Am. Chem. Soc.* **2009**, *131*, 15647. (c) Toher, C.; Rungger, I.; Sanvito, S. *Phys. Rev. B* **2009**, *79*, 205427.